Article

Biosensor Enhancement Using Grooved Micromixers: Part I, Numerical Studies.

Nicholas Scott Lynn Jr., and Jiri Homola

Anal. Chem., **Just Accepted Manuscript** • DOI: 10.1021/ac504359m • Publication Date (Web): 07 Apr 2015

Biosensor Enhancement Using Grooved Micromixers: Part I, Numerical Studies

N. Scott Lynn Jr., Jiří Homola*

Institute of Photonics and Electronics, Academy of Sciences of the Czech Republic
Chaberská 57, Prague, Czech Republic

*Corresponding Author
Jiří Homola
homola@ufe.cz
Chaberská 57
Prague, Czech Republic

Abstract

In this study we examine the use of the staggered herringbone mixer (SHM) to increase the efficiency of analyte delivery to a planar biosensor surface. Although there has been an extensive amount of research regarding the optimization of the SHM for mixing purposes, there has been very little work regarding the use of said micromixers for sensing purposes. Here, we use numerical methods to examine the effect of the SHM geometry on the efficiency of analyte delivery to a biosensor surface. We show the level of sensing enhancement of an SHM-based sensing chamber over that of an unmixed chamber has a strong dependence on the SHM geometry, the Péclet number, and the overall sensor length. The results presented herein are applicable to a very wide range of biosensor transduction mechanisms and target analytes.

Introduction

Over the past 30 years, affinity-based biosensing technologies have become increasingly prevalent as analytical devices, providing an invaluable tool for diagnostic, analytic, and research purposes.[1] Despite having a wide range of biocomponents and transduction mechanisms, affinity biosensors generally work via the same principle: a signal change is observed after an immobilized biocomponent acts to capture a target analyte, delivered to the sensor surface through convective and diffusive means.[2] These sensors are often operated in the mass-transfer limited regime, where the rate of change of the sensor response is proportional to the rate of analyte delivery to the sensor surface. An increase in the efficiency of this analyte delivery will result in a sensor with a higher sensitivity, and furthermore, a lower limit of detection.

There has recently been a rise in the use of biosensors utilizing microfluidic means of analyte delivery.[3] A large proportion of these biosensors are operated such that the interaction between capture probe and analyte is mass-transfer limited, resulting in the formation of an analyte boundary layer that acts as a resistance to analyte capture. In this regime, rates of analyte delivery can be increased with increases in the volumetric flow rate Q (scaling as $Q^{\frac{1}{3}}$),[4] or by decreases in the channel height H_c (scaling as $H_c^{-\frac{2}{3}}$),[5] where both methods have finite limitations. Other methods to increase rates of analyte delivery include the fluidic removal of the depleted layers[6] or by sheathing the fluid closer to the sensor,[7] both coming at the expense of increased fluidic complexity. Recently, multiple authors have explored the use of microfluidic mixing strategies to reduce the size of the depletion layer and enhance the sensor performance. Several active mixing strategies have been used for sensing purposes, including the use of electrothermal stirring,[8] AC electro-osmotic flow,[9] and the use of magnetic beads.[10]

The staggered herringbone mixer (SHM) is a passive mixer that has been shown to mix fluids via Lagrangian chaos, providing an effective mixing profile that is independent of the Reynolds number (Re < 1).[11] The overall design of the SHM and its potential use as a tool for biosensor enhancement is shown in Fig. 1. A series of herringbone shaped grooves on the topside of the microchannel serve to stir the fluid in a bihelical profile. If designed correctly, this additional fluid motion will serve to deliver fresh analyte to the sensor surface situated on the opposite plane of the grooves. There have been a large number of studies involving the optimization of this device for mixing purposes;[12-19] however, the amount of research concerning the optimization of the SHM for the enhancement of mass transfer is more limited.

In the seminal paper on this topic, Kirtland and Stroock developed an analytical solution to approximate SHM-type flow in a simple rectangular channel. This solution was then used to study the influence of the mass transfer Péclet number (Pe) on the efficiency of mass transfer to a sensor surface, characterized by the Sherwood number (Sh).[20] For a rectangular, chaotically stirred channel with constant normalized transverse velocity, they demonstrated that for sufficiently long channels the Sherwood number deviated from the behavior of an unstirred channel to asymptotic value Sh_∞ that scaled as $Sh_\infty \sim Pe^{1/3}$ for Pe > 500. Conversely, the system displayed characteristics similar to that of an unstirred channel as $Pe \to 0$. Unfortunately, the geometry of the SHM is much more complex than a standard rectangular microchannel, where axial and transverse fluid velocities will rise and fall in a complex periodic fashion in the regions under the ridges and grooves, respectively.

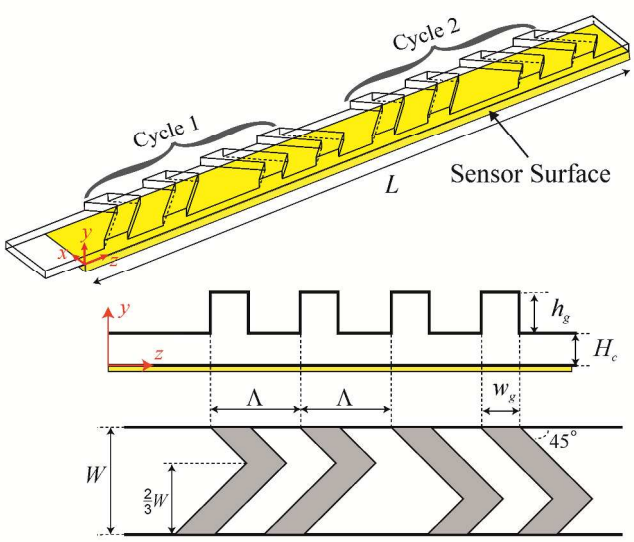

Figure 1. Parameters associated with the SHM-sensor used in this study.

Experimentally, the use of the SHM for biosensing enhancement purposes has been limited to a handful of papers. Foley *et al*. used a computational model to simulate the sensor response of flow in a 1.5 mm long channel having SHM-type V-grooves for the capture of streptavidin; they predicted no sensor enhancement over an unmixed channel (Pe = 134).[21] Golden *et al*. used a grooved micromixer in a 140 mm long microchannel for a biotin-avidin immunoassay, showing an enhancement of 1.26-1.46 (26-46%) over an unmixed channel (Pe ~ 1000).[22] In another experiment, Wang *et al*. used a 800 mm long microchannel for the capture of circulating tumor cells (CTCs), where an increase in the cell capture yield of 1.63 (63%) was seen between the SHM and an unmixed channel ($Pe = 10^6$).[23] Finally, Stott *et al*. used a SHM of length ~25 mm for the capture of various CTCs to see an increase in capture yield of 2.72 (172%) with respect to a unmixed channel ($Pe > 5\times10^6$), with larger increases between

the two with increasing flow rate;[24] although in that study the unmixed channel had a larger effective height with respect to the SHM-based channel. It should also be noted that Stott *et al*. used the entire SHM-surface for analyte capture (including surfaces of grooves); this case is different from the other previous works (and the results presented here), which deal with the transfer of analyte to the surface opposite the SHM-grooves.

These results, as well as the predictions by Kirtland and Stroock, highlight the importance of the Péclet number and channel length on any sensor using grooved microchannels for the enhancement of a biosensing process. Of further importance is how the geometrical parameters in Fig. 1 influence the rate of mass transfer to the sensor surface. Forbes and Kralj examined the influence of these parameters on the frequency of fluid streamline interactions with a variety of surfaces related to the SHM;[25] however, it has not been established how these streamline-surface interactions relate to the convection, diffusion, and capture of analyte. To date, there has been no detailed exploration on how the geometrical (groove and channel geometries) and operational (flow rate, analyte diffusivity) parameters associated with the SHM influence the enhancement of mass transfer to a biosensor surface.

In this study we examine how the groove width (w_g), pitch (Λ), groove height (h_g), channel height (H_c), channel width (W), number of grooves per ½-cycle (N_g), and sensor length (L) influence the efficiency of mass transfer between the bulk fluid and the sensor surface for a sensor utilizing the SHM for enhancement purposes. As in the study by Kirtland and Stroock, we characterize the efficiency of mass transfer via the Sherwood number. Sensors characterized as having a higher Sherwood number will collect analyte with a higher efficiency, and therefore, will possess better overall sensing characteristics. The level of enhancement that a sensor will gain via microfluidic mixing is related to the difference between the characteristic Sh values between the mixed and unmixed cases. We discuss what levels of enhancement can be expected when using the SHM for biosensing purposes, and how those levels of enhancement depend on the Péclet number. The results of this study are directly applicable to a wide range of biosensing platforms, and can be used as a guide for the design of appropriate microfluidic sensing chambers.

Analyte Capture via Stirred Flows

The enhancement of mass transfer is best described by the ratio of the analyte binding rate to the sensor surface between an SHM-mixed channel and that of an unmixed channel of height H_c. The choice of a reference channel of height H_c (as opposed to the height of the full channel $H_c + h_g$) allows

for a mixed and unmixed sensor chamber to have the same Péclet number when presented with target solutions having the same volumetric flow rate Q (representing an average inlet fluid velocity U). We define the Péclet number as $\mathrm{Pe} = UH_c/D$, where D is the diffusivity of the target analyte.

The response of a biosensor to the presence of an analyte within a mixed flow cell is a complex topic, involving the unsteady state convection, diffusion, and capture of analyte by the sensor surface. Despite this complexity, the problem can be simplified with the assumption that the sensor is operated in the mass transfer limited regime, where rates of analyte capture are much greater than the rates of convective and diffusive transport of analyte to the sensor surface. We can also assume that the concentration of analyte C is sufficiently low such that changes in the analyte boundary layer shape during the assay occur slowly enough that the assay is quasi-steady (relevant for most affinity-based assays).[4] Under these two assumptions, the distribution of analyte in the sensing chamber resembles that of the steady-state solution for analyte flowing through the sensing chamber with a condition of $C = 0$ on the sensor surface. Therefore, the problem can be reduced to finding the ratio of the steady state analyte flux J between a SHM-based sensing chamber geometry (Fig. 1) and that of a simple rectangular channel. From a computational perspective, the fluid velocity and pressure field through the SHM can be solved with high accuracy using a variety of methods.[12-17] Unfortunately, accurate solutions for the analyte concentration field can only be obtained for very short sensing chambers: the presence of numerical (false) diffusion require the use of unrealistically high mesh densities.[26]

To avoid this problem, we utilize a particle tracing method similar to that employed by Kirtland and Stroock.[20] Briefly, after obtaining the solution for the velocity field (using the finite element method), we track the advection of a series of tracer particles through the SHM domain, where at each time-step we add a random displacement in each direction. The particle is removed from the flow if it interacts with the sensing surface, where the position of interaction is recorded. This method allows for the discrete computation of the steady-state mixing cup concentration C_b throughout the sensor. From the conservation of mass, the analyte flux to the sensor can then be calculated as

$$J = UH_c\, dC_b/dz. \quad \textbf{(1)}$$

From a mass-transfer perspective, the efficiency of analyte capture in a microfluidic biosensor is best characterized by the Sherwood number,[27] $\mathrm{Sh} = kH_c/D$, where k is the mass transfer coefficient, and H_c has been chosen as the characteristic length of the system. For a mass transfer limited system the analyte flux can be described as $J = -kC_b$, and Sh can be calculated as

$$\mathrm{Sh} = -\frac{JH_c}{C_b D} = \frac{-\mathrm{Pe}H_c}{C_b}\frac{dC_b}{dz} = -\frac{d\ln C_b}{d\bar{z}}\ , \qquad (2)$$

where $\bar{z} = z/\mathrm{Pe}H_c$ is the dimensionless axial distance (known as the inverse Graetz number).[20]

The sensing chambers considered here entail flow within a rectangular channel (with or without grooves), with one side of the channel acting as a reactive surface for analyte capture. In the laminar flow regime, all *unmixed* sensors of this type (rectangular cross-section) will exhibit the same characteristic Sh vs. $\bar{z}$ curve, regardless of the Péclet number or the channel aspect ratio (save for the extreme limits of $H_c/W >> 1$, which is not an ideal sensor design). This curve (shown in Fig. 2C) has two distinct characteristics. In the entrance region ($\bar{z} < 0.01$) the analyte boundary layer is thin with respect to H_c, and the Sherwood number is proportional to $\bar{z}^{-1/3}$. In the fully developed region at axial distances of approximately $\bar{z} > 0.2$, the analyte boundary layer has filled the channel and the Sherwood number approaches a constant value of 2.55.

Fortunately, the characteristic Sh on $\bar{z}$ behavior for a *chaotically mixed* sensor will exhibit traits that are very similar to that of an unmixed channel. These traits have been explored by Kirtland and Stroock and are summarized here: [20]

i. Similar to an unmixed system, a mixed sensor will have an entry region with the Sherwood number scaling as $\mathrm{Sh} \propto \bar{z}^{-1/3}$. This region will persist for a finite length z_∞ that is proportional to the inverse characteristic transverse fluid velocity u_t, where $z_\infty \sim WU/u_t$.

ii. For chaotically mixed flows in rectangular channels, Sh will deviate from the entry region to an asymptotic value of Sh_∞ at axial lengths of $z > z_\infty$, where $\mathrm{Sh}_\infty \geq 2.55$. The term z_∞ is the asymptotic length of the mixer, where increases of z beyond this limit do not result in any changes to Sh.

iii. This asymptotic behavior is at the mercy of how the fluid is mixed, as there will be a slow decrease in Sh ($z > z_\infty$) for non-chaotically mixed fluids.

iv. The magnitude of Sh_∞ will increase monotonically with the Péclet number. At lower Pe values the system will resemble that of an unmixed system, with $\mathrm{Sh}_\infty \to 2.55$.

Therefore, in order to find the asymptotic Sherwood number for a given chaotically-mixed sensor geometry, we only need to simulate the behavior of a sensor that is sufficiently longer than the critical transition length z_∞. After the asymptotic value of Sh_∞ is obtained, the characteristic dimensionless response can be estimated via a smooth transition between the theoretical Sh vs. $\bar{z}$ response for an

unmixed sensor for values of $z < z_\infty$ and a constant value of Sh_∞ for $z > z_\infty$ (details in the SI). In this study we assume that z_∞ can be calculated from the intersection of Sh_∞ with the unmixed Sh vs. $\bar{z}$ data. From Eqn. 2, the values for C_b for a mixed system can then be calculated as

$$\int_{C_o}^{C_b} d\ln(C_b) = \int_{z=0}^{z} \frac{-\mathrm{Sh}}{\mathrm{Pe} H_c} dz, \quad \textbf{(3)}$$

where the choice of the inlet analyte concentration C_o is arbitrary when comparing a mixed sensor to a unmixed sensor. Finally, the analyte flux is calculated via substitution of Eqn. 2 into Eqn. 1 as

$$J = \frac{\mathrm{Sh} C_b D}{H_c}. \quad \textbf{(4)}$$

Assuming both the sensor is interrogated along the entire length and the sensor has a linear response to the binding of analyte, we can estimate the analyte flux to the sensor using the average value of J within the region $0 \le z \le L$. The sensing enhancement (E_{mix}) can then be represented by the ratio of the average analyte flux between a SHM-based sensor J_{mix} and an unstirred channel J_{ref}. Henceforth, this study is comprised of two components, the first being an analysis of the effects of the SHM geometry on Sh_∞ at a constant Péclet number, and the second being an analysis of the effects of the Péclet number on both Sh_∞ and E_{mix} for an optimized SHM geometry.

Results and Discussion

Calculation of the Sherwood Number. Details on the numerical methods used in this study can be found in the SI. Briefly, we utilized a finite element package (COMSOL) to calculate the fluid velocity and pressure throughout a SHM domain. We then used COMSOL to simulate the advection and diffusion of a series of particles through the same domain, where a particle was considered captured if it made contact with the sensor surface. The locations of these captured particles allow for the calculation of C_b and Sh (via Eqn. 2) as a function of z throughout the domain.

For purposes of convenience, we define a base geometry with dimensions that are commonly found in both biosensing and SHM literature, with W = 200 μm, H_c = 20 μm, h_g = 20 μm, Λ = 150 μm, and N_g = 2. All simulations were conducted with constant average fluid velocity of U = 5 mm/s, with modification to the Péclet number through the analyte diffusivity D. There was no significant difference in simulation outcomes by keeping D constant while varying U.

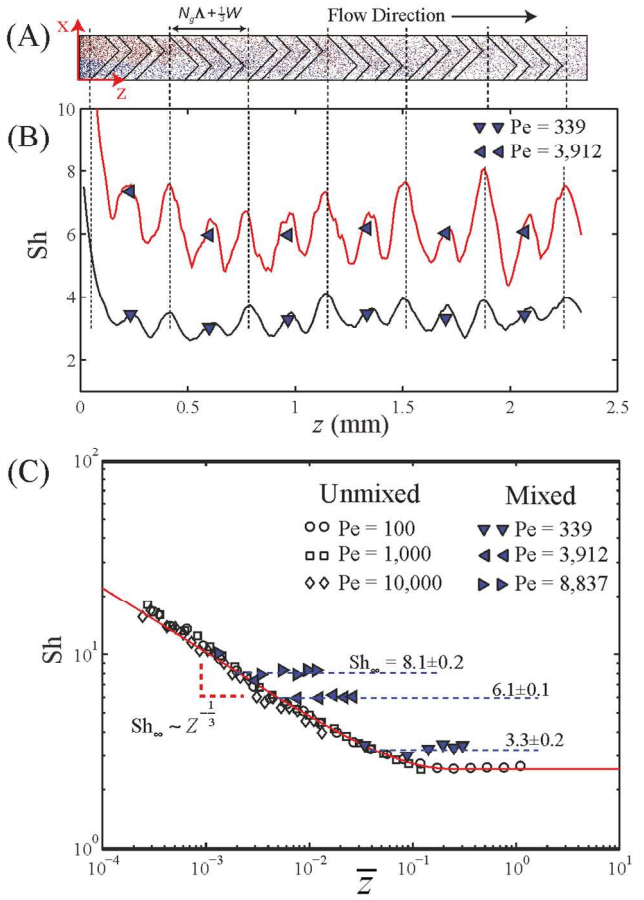

Figure 2. (A) Captured particle positions for the base geometry with Pe = 339 ($D = 2.94\times10^{-10}$ m^2/s). The particles are colored according to their seeded *x*-position. (B) Sh vs. *z* for two Pe values for the base geometry. The solid red lines were calculated using 300 equidistant planes at constant *z*-positions. The symbols were calculated using 7 planes separated by a distance $N_g\Lambda+\frac{1}{3}W$ (indicated by the dashed lines). (C) Sh vs. $\bar{z}$ for both an unmixed reference sensor as well as the base geometry SHM. The red line shows the theoretical behavior of an unmixed sensor (details of calculation in SI).

Figure 2A displays the captured particle positions along the sensor floor regarding flow through the SHM base geometry (Pe = 339). The captured particle positions represent a discrete approximation to the steady-state diffusive analyte flux *J* to the sensor surface, with *J* being proportional to the surface density of captured particles. There are several noticeable trends within the figure (high resolution image available in the SI): it can be seen that there is an overall decrease in the particle density with increasing *z*; a localized decrease in the density under the position of each groove; and a localized increase in the density downstream of each groove apex. These trends mirror the low Pe number simulations performed by Foley *et al*. via the direct unsteady-state solution to the convection-diffusion equation.[21] Using a series of equally spaced planes of constant *z*, these particle positions can be used to calculate an estimate for C_b, which can then be used to calculate Sh via Eqn. 2.

Figure 2B displays Sh as a function of *z* for two different Péclet numbers regarding the base geometry. As expected, the plots of Sh vs. *z* oscillate in a periodic manner, with increased and

decreased Sh values in the cross-sectional channel areas where the grooves are more and less prevalent, respectively. This oscillation is due to several reasons. Firstly, the localized values of J are higher in the regions immediately downstream of each groove, where the channel undergoes an overall height of $H_c + h_g$ (under each groove) to a height H_c.[4, 5] Secondly, each groove acts to transport a portion of the fluid in the channel cross-section across the channel width. The flow within each groove has a swirling motion transverse to the local axis of the groove, provided the grooves are sufficiently deep.[18] This flow thus acts to bring fresh analyte to the sensor surface and results in higher values of J in regions near the apex of each groove structure. This spatial dependence of J (and Sh) along the sensor length can be visualized using steady-state finite element solutions of the convection-diffusion equation (included in the SI). It should be noted that these are only qualitative solutions due to the aforementioned problems with numerical diffusion.

The differences between a mixed and unmixed sensing chamber can be distinguished by the examination of the behavior of Sh as a function of the dimensionless axial distance $\bar{z}$. Figure 2C compares the Sh vs. $\bar{z}$ behavior between an unmixed reference sensor and that of the base geometry shown in Fig. 2B for three different Pe values. The discrete data for the unmixed channel were calculated using 25 logarithmically spaced z-positions. For purposes of comparison, we calculated the Sh vs $\bar{z}$ response of a 2D, unmixed sensor via the solution of the convection-diffusion equation at low Pe, which is shown in the solid red line (details in the SI). The independence of Pe regarding the calculation of Sh vs. $\bar{z}$ for unmixed sensors can be seen here, as the discrete Sh vs. $\bar{z}$ data calculated for three different Pe values closely match the data provided by the continuous solution. The data shown in Fig. 2 serve to verify the particle tracing method used here.

The discrete solutions for the SHM base geometry channels highlight the Sh vs. $\bar{z}$ behavior of mixed sensing chambers. It can be seen that the SHM-mixed channel approaches asymptotic values of Sh_∞ = 3.3 ± 0.2, 6.1 ± 0.1, and 8.1 ± 0.2 for Péclet numbers of Pe = 339, 3912, and 8837, respectively. The transition to the asymptotic region for all three Péclet numbers occurs before the 2nd groove ½-cycle (z = 367 μm). It is a safe assumption that the base geometry will generate a chaotic mixing profile (discussed below); therefore, it is also reasonable to assume that the Sh value will not degrade for larger sensing domains. In this study we report Sh_∞ as the mean ± standard deviation of the average Sh value from the 2nd to the last symmetry plane in the simulation. The values of Sh_∞ reported here were taken from a minimum of 5 groove ½ cycles, where the total number of full cycles (N_c) was such that $N_c \geq 3$ (limited by available computational memory).

Effect of channel width. The results shown in Fig. 2 regard the base geometry, with no changes to the geometric parameters that describe the herringbone grooves. It is important to know how these parameters affect the asymptotic Sherwood number. For this portion of the discussion we will restrict the analysis to systems having Pe = 5125; the effect of Pe on Sh_∞ will be discussed later.

In a previous study involving stirred flow in a rectangular channel, Kirtland and Stroock showed that in a mixed rectangular channel, the asymptotic Sherwood number is related to the magnitude of the transverse velocity u_x, where $\mathrm{Sh}_\infty \sim (u_x/U)^{1/3}$.[20] Likewise, it has been shown that for a given channel design (constant W, H_c, H_g, Λ), there exists an optimum value of w_g such that the normalized transverse velocity u_t/U is maximized.[16] Therefore it is reasonable to expect that there exists an optimum w_g that maximizes Sh_∞.

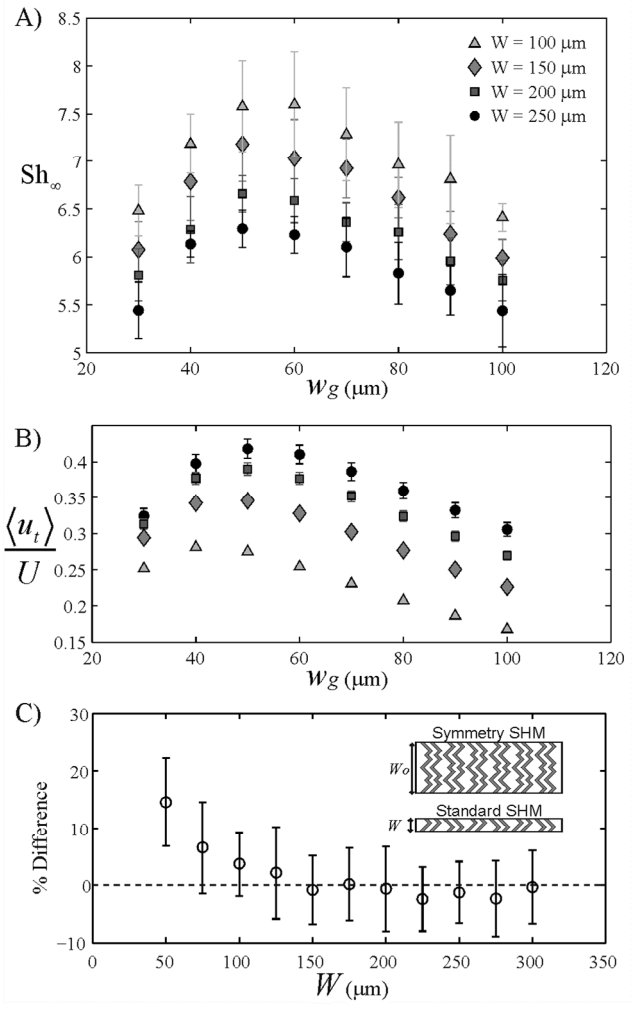

Figure 3. (A) Asymptotic Sherwood number plotted against the groove width w_g, with varying channel width W (H_c = 20 μm, h_g = 20 μm, Λ = 150 μm, N_g = 2). (B) Normalized transverse velocity vs. the groove width regarding the data shown in Fig. 3A. (C) Percent difference of a symmetry solution vs. a non-symmetry solution vs. W for the base geometry SHM (base geometry H_c = 20 μm, h_g = 20 μm, Λ = 150 μm, w_g = 60 μm, N_g = 2)

Figure 3A plots the asymptotic Sherwood number versus w_g for a variety of channel widths (constant H_c, h_g, Λ, N_g). It can be seen that Sh_∞ increases with decreasing W, and the optimum value of w_g that maximizes Sh_∞ is relatively constant for each W. Figure 3B plots the normalized transverse velocity regarding flow in the SHM vs w_g for the same simulations shown in Fig. 3A (details in the SI). Unlike the results shown in Fig. 3A, there is a clear shift in the value of w_g that optimizes the transverse velocity: at W = 100 μm the asymptotic Sherwood number is maximized at a value of $w_g \approx 40$ μm, whereas at W = 250 μm Sh_∞ is maximized at a groove width in the range of 50-60 μm. Interestingly, it can be seen that values of u_t/U increase with increasing W, whereas Sh_∞ increases with decreasing W; a trend that is not seen for mixed flows in simple rectangular channels.[20]

These data also contradict the optimal w_g to maximize streamline surface interactions predicted by Forbes and Kralj.[25] In that study, the optimal w_g for the interactions between fluid streamlines and the entire SHM surface was predicted via the groove width that equalized the viscous resistance of flow in the main channel (defined by W and H_c) and the transverse flow within the groove (defined by w_g and h_g). Using their methods, the optimum w_g values for the results in Fig. 3A should increase linearly with W, having predicted values of w_g = 73 μm, 107 μm, 141 μm, and 175 μm for channel widths of W = 100 μm, 150 μm, 200 μm, and 250 μm, respectively. Conversely, the data shown in Fig. 3A show that the optimal groove width (for Sh_∞) increases only slightly with increasing channel width. Although their study was directed towards *all surfaces* of the SHM acting to capture analyte, they reported similar optimal w_g values between the entire SHM surface and the surface of interest in this study.

Fig. 3A shows that the asymptotic Sherwood number increases when the width of the microchannel decreases. Although this increase in Sh_∞ is desired, very low values of W might be detrimental in a sensing format (e.g. loss of signal with decreased sensing area) and also may be difficult to fabricate. For sensing applications the concentration of analyte is homogenous across the cross-section at the sensing chamber inlet and mixing of the fluid across that same width is not required. Therefore, herringbone designs can be placed side by side in a symmetric fashion to accommodate the footprint of the sensing mechanism (with an overall width W_o), keeping the benefits of smaller herringbone structures while maintaining a larger overall channel width. In this case the only changes to the simulations shown in Fig. 3A and B would be a symmetry boundary condition on the channel sidewalls rather than a no-slip condition. Figure 3C plots the %-difference between a symmetry

boundary condition ($\mathrm{Sh}_{\infty,symm}$) and the no-slip boundary condition vs. the channel width. It can be seen that as W increases the difference between the symmetry and non-symmetry solutions approaches zero; the increase in $\mathrm{Sh}_{\infty,symm}$ at low W is attributed to the lack of viscous interaction of the fluid with the channel sidewalls. This increase in $\mathrm{Sh}_{\infty,symm}$ demonstrates a method to increase the efficiency of a sensing system (decreasing W with constant W_o) while maintaining higher mass transfer rates in a larger sensing footprint.

Effect of groove height. The height of the grooves has been shown to be one of the most important parameters regarding an SHM used for mixing purposes.[16-19] The overall rate of transverse flow has been shown to increase with increasing h_g, where above the limit of $h_g/H_c \approx 2$, the overall rate of transverse flow in the channel becomes constant.[16] Figure 4A plots Sh_∞ vs w_g for a channel design with varying h_g. As expected, it can be seen that Sh_∞ increases monotonically with h_g for all values of w_g. In addition, the optimal groove width increases from w_g = 40 μm to 70 μm for h_g = 10 and 40, respectively.

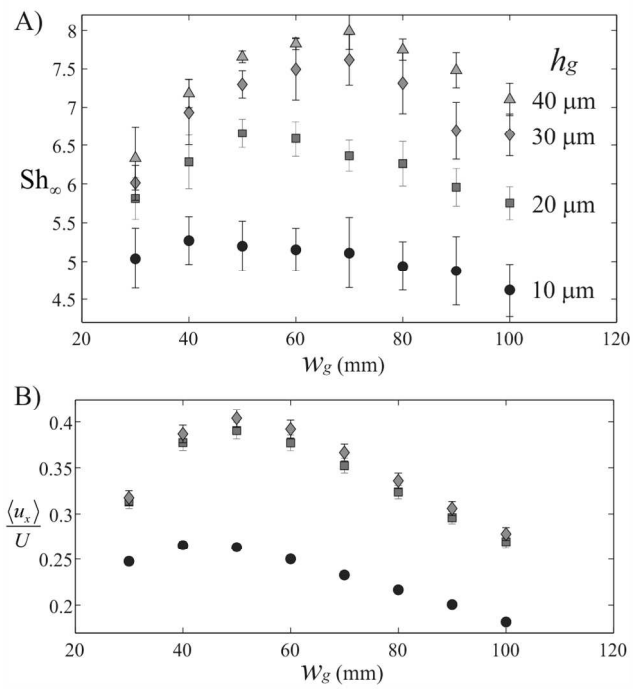

Figure 4. (A) Asymptotic Sherwood number plotted against w_g with varying groove height h_g (H_c = 20 μm, W = 200 μm, Λ = 150 μm, N_g = 2). (B) Normalized transverse velocity vs. w_g regarding the data shown in Fig. 4A (data for h_g = 40 μm are not shown).

Figure 4B displays the normalized transverse fluid velocity vs. w_g for the data shown in Fig. 4A. Increases of u_t/U can be seen with increasing h_g; however, the rates of transverse velocity reach a

maximum at h_g = 30 μm (the data for h_g = 40 μm are indistinguishable from h_g = 30 μm, and are not shown). As seen in the data presented in Fig. 3, the values of u_t/U and Sh_∞ are maximized at different groove widths. This suggests that the $\mathrm{Sh}_\infty \sim u_x^{1/3}$ scaling law, although accurate for stirred flows in rectangular geometries, is not directly applicable to the complex geometry of the SHM. Furthermore, the data in Fig. 4 also contradict the results of Forbes and Kralj,[25] where using their methods the optimal groove spacing for this channel design can be calculated as w_g = 420, 141, 83, and 62 μm for h_g = 10, 20, 30 and 40 μm, respectively. The results shown in Figs. 3 and 4 were calculated at a Péclet number of 5125, well within the convection dominated regime. We found no difference in the optimal groove width in the range of Pe > 100. The difference between the results shown here and those shown by Forbes and Kralj[25] highlight the importance of diffusion, however small, for the capture of an analyte by a sensor surface in complex microchannel geometries such as the SHM. The SHM provides a flow having a chaotic nature where two streamlines situated near one another at the channel inlet will eventually be separated at some downstream axial distance. Because the process of diffusion allows an analyte to move across these streamlines, it must be taken into account when dealing with any mass-transfer process.

Other geometric considerations. We have also studied the influence of the groove pitch Λ and the number of grooves per half-cycle N_g. We found that both Λ and N_g have small effect on Sh_∞; the details regarding these two parameters can be found in the SI.

Effect of Péclet number. The results discussed in the previous section entail how the mass transfer efficiency of a SHM change with a variety of parameters at a constant Péclet number. At this point, the effect of Pe on the Sherwood number regarding a SHM used for sensing purposes is unknown.

Figure 5A shows Sh_∞ vs. Pe regarding three mixers having varying h_g in the range of $10^2 < \mathrm{Pe} < 10^4$. All three SHM designs follow a $\mathrm{Sh}_\infty \sim \mathrm{Pe}^{\frac{1}{3}}$ scaling law at high values of Pe, where the transition to this regime is dependent on h_g (each SHM design tested follows this trend). Additionally, it can be seen that $\mathrm{Sh}_\infty \to 2.55$ for low values of Pe, seen here specifically for the shallow groove SHM (h_g = 5 μm). This behavior at low Pe is also seen for chaotically mixed flows in a simple rectangular channel with constant u_t/U.[20] This behavior for a SHM-based channel is rather interesting when considering the fact that the effective channel height (and overall velocity magnitude) is not constant along the channel axis within the SHM.

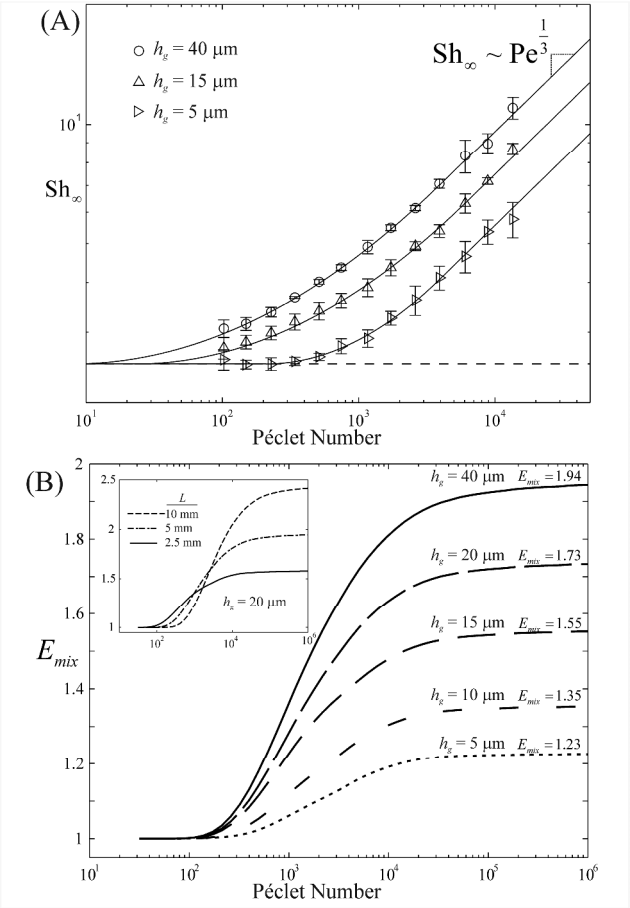

Figure 5. (A) Asymptotic Sherwood number vs. Péclet number for an SHM (W = 200 μm, H_c = 20 μm, Λ = 150 μm, w_g = 60 μm, N_g = 2) with varying h_g. The dashed line represents a value of $\mathrm{Sh}_\infty = 2.55$. (B) Sensor enhancement E_{mix} vs. Péclet number regarding the SHM in Fig. 5A with varying h_g, for a sensor with L = 5mm. *inset*: E_{mix} vs. Pe for a sensor with h_g = 20 μm having varying sensor length L.

From the data shown in Fig. 5A, it is clear that there will be an enhancement in mass transfer in sensors utilizing the SHM at high Péclet numbers. Although these data are useful, Sh_∞ does not provide any information regarding the specific sensing enhancement the SHM might provide; for this purpose information on the analyte flux or analyte binding rate to the sensor is required. In order to obtain this information, a smooth curve was fit to the Sh_∞ vs. Pe data consisting of (*i*) a power law fit of the type $\mathrm{Sh}_\infty \sim \mathrm{Pe}^{\frac{1}{3}}$ in the range of $\mathrm{Pe} > 3000$, and (*ii*) a 2nd order polynomial (to the log-log data) having a zero slope at $\mathrm{Sh}_\infty = 2.55$ with a matching slope and absolute value to the former power law fit where the two regions meet. These fits are shown as the solid lines in Fig. 5A, where every fit in this study has a coefficient of determination such that $R^2 > 0.97$. Given a specific Pe, the fits shown in Fig. 5A were then used to construct a smooth Sh vs. $\bar{z}$ relationship regarding a mixed system (as shown in Fig. 2C), which was then used to calculate the average analyte flux J_{mix} to the mixed sensor for an

analyte concentration C_o using Eqns. 3 and 4. The sensing enhancement is then calculated as $E_{mix} = J_{mix}/J_{ref}$, where J_{ref} is the average analyte flux to an unmixed sensor calculated using the same methods. Details on these calculations are in the SI. We utilize this form of E_{mix} due to its direct relationship on the enhanced performance of a SHM-based sensor with respect to a channel of height H_c. With respect to an unstirred channel, the analyte binding rate for a mixed system will scale proportionally to E_{mix}, and the sensor limit of detection (LOD) will scale as E_{mix}^{-1}.

Figure 5B plots E_{mix} vs. Pe for an SHM design having a length of L = 5 mm and varying h_g. The effect of the Péclet number on the sensing enhancement is clear, where it can be seen that $E_{mix} \to 1$ for low Pe, and E_{mix} increases to an asymptotic maximum at high Pe, where the maximum value of E_{mix} increases monotonically with h_g (following the increase of u_t/U with h_g).

The sensing enhancement is also strongly dependent on L. There will be no net enhancement for sensor lengths of $L < z_\infty$, where the response of a mixed sensor follows that of an unmixed sensor. For SHMs having sufficiently deep grooves (ensuring enough fluid recirculation), this critical distance can be smaller than the length of the 1st ½-cycle. For sensors with $L > z_\infty$ there will be an initial increase in E_{mix} with increasing L, which is evident from the Sh vs. $\bar{z}$ relationship shown in Fig. 2C, where the difference between the Sherwood number for mixed and unmixed systems increases asymptotically with increasing $\bar{z}$ ($z < z_\infty$). An example of this dependence is shown in the inset of Fig. 5B, which plots E_{mix} vs. Pe for three different sensor lengths. It can be seen that the maximum value of E_{mix} increases with increasing L, which is followed by an increase in the critical Pe above which there exists a net sensor enhancement. The maximum enhancement values for the inset in Fig. 5B are E_{mix} =1.4, 1.73, and 2.14 for sensor lengths of L = 2.5, 5, and 10 mm. It should be noted that this relationship cannot continue indefinitely; for very long channels such that all of the analyte is collected (in both mixed and unmixed channels), the binding rates for both channels will be equivalent, where $E_{mix} \to 1$. The details of this behavior are discussed in part II of this study.[28]

The ramifications of using an SHM for sensing purposes can be drawn from the results shown in Fig. 5. Not only does the overall geometry of the herringbone grooves carry significant importance, but the experimental outcomes are also strongly dependent on the length of the mixer as well as the experimental conditions in use (flow rate, diffusivity of analyte). This can lead to variable results when using grooved mixers when no regard is given to the details of the effects discussed above. This is noticeably seen in the previous experimental results on this topic, where experimental measurements

ranged from E_{mix} = 1 (L = 1.5 mm, Pe = 134, Foley *et al*.)[21] to E_{mix} = 1.63 (L = 800 mm, Pe = 1,200,000, Wang *et al*.).[23]

Given an experimental system incorporating the SHM while having pre-defined operating conditions, the choice of analyte can have strong implications. For example, using a 5mm long SHM designed with the base geometry (Fig. 5B, h_g = 20 μm) operated in a symmetric fashion with overall width W_o = 1 mm and a flow rate of Q = 1 uL/min (U = 0.83 mm/s), the choice of analyte will determine the effectiveness of the SHM for sensing enhancement: the detection of (*a*) 11-mer ssDNA ($D = 9\times10^{-11}$ m^2/s, Pe = 184) will yield an enhancement of $E_{mix} \approx 1$, whereas the detection of (*b*) whole cell bacteria (1 μm diameter, $D = 3.2\times10^{-13}$ m^2/s, Pe = 51,875) will yield an enhancement of $E_{mix} = 1.7$, a rather large difference considering the user might have expected similar enhancement values.

If desired, the parameter E_{mix} can easily be measured experimentally, for example, by using a real-time, label-free biosensor and comparing the binding rates between a SHM-based channel and an unstirred reference channel. In this case the SHM can be fabricated using the multilayer deposition of a thick-film photoresist (e.g. Su8), after which the sensing chamber can be fabricated by sealing the open face channel to the sensing surface. These experiments are the focus of part II of this study, which regards the experimental verification of the methods and results shown herein.[28]

Conclusions

These results highlight the regimes in which the staggered herringbone mixer (SHM) can be used to enhance the performance of a microfluidic based affinity biosensor. The results in this study are applicable to sensors using the SHM for enhancement of mass-transfer towards the surface situated opposite the mixing grooves. Specifically, we characterized changes to the herringbone structure geometries via their effect on the asymptotic Sherwood number Sh_∞, which relates the efficiency of analyte mass transfer to the sensor surface. We have found that there is an optimum groove width w_g that maximizes Sh_∞ regarding a SHM having set channel height H_c, groove pitch Λ, groove depth h_g, and number of grooves per ½-cycle N_g; these optimum values of w_g contradict those found in a previous study involving the optimization of fluid streamlines to the channel walls of the SHM.[25] Using an optimized SHM design we then examined the effect of the Péclet number on Sh_∞, and we have also predicted the level of enhancement E_{mix} of a SHM-based sensor with respect to an unstirred channel. Our results predict a strong dependence on both Pe and the sensor length L for a specific SHM design. These results are consistent with the experimental findings by three previous authors.[21-23]

The results of this study are specific to mass-transfer limited sensors, which encompass a large portion of biosensors within the present literature.[4] Because of the strong dependence of E_{mix} on Pe, care must be taken to ensure the sensor is operated under conditions of high Pe. On this note, the use of the SHM for biosensing enhancement is most beneficial for the detection of analytes having low diffusivity, such as large proteins, viruses, and cells. Although a search for an upper limit of E_{mix} was not carried out, these results make clear that the use of the SHM will provide an enhancement limited to within an order of magnitude with respect to an unmixed sensor of equivalent height. The experimental verification of these results is the focus of part II of this study.[28]

Acknowledgements

This research was supported by Praemium Academiae of the Academy of Sciences of the Czech Republic and the Czech Science Foundation (contract # P205/12/G118).

Supporting Information

Additional information as noted in text. This information is available free of charge via the Internet at http://pubs.acs.org.

References

1. A. P. F. Turner, *Chemical Society Reviews*, 2013, 42, 3184-3196.
2. K. R. Rogers, *Molecular biotechnology*, 2000, 14, 109-129.
3. S. Prakash, M. Pinti and B. Bhushan, *Philos T R Soc A*, 2012, 370, 2269-2303.
4. T. M. Squires, R. J. Messinger and S. R. Manalis, *Nature Biotechnology*, 2008, 26, 417-426.
5. N. S. Lynn, H. Sipova, P. Adam and J. Homola, *Lab on a Chip*, 2013, 13, 1413-1421.
6. S. K. Yoon, G. W. Fichtl and P. J. A. Kenis, *Lab on a Chip*, 2006, 6, 1516-1524.
7. O. Hofmann, G. Voirin, P. Niedermann and A. Manz, *Analytical Chemistry*, 2002, 74, 5243-5250.
8. M. Sigurdson, D. Z. Wang and C. D. Meinhart, *Lab on a Chip*, 2005, 5, 1366-1373.
9. R. Hart, R. Lec and H. Noh, *Sensor Actuat B-Chem*, 2010, 147, 366-375.
10. P. Kinnunen, I. Sinn, B. H. McNaughton and R. Kopelman, *Appl Phys Lett*, 2010, 97.
11. A. D. Stroock, S. K. W. Dertinger, A. Ajdari, I. Mezic, H. A. Stone and G. M. Whitesides, *Science*, 2002, 295, 647-651.
12. T. G. Kang and T. H. Kwon, *J Micromech Microeng*, 2004, 14, 891-899.
13. H. Z. Wang, P. Iovenitti, E. Harvey and S. Masood, *J Micromech Microeng*, 2003, 13, 801-808.
14. D. G. Hassell and W. B. Zimmerman, *Chem Eng Sci*, 2006, 61, 2977-2985.
15. J. T. Yang, K. J. Huang and Y. C. Lin, *Lab on a Chip*, 2005, 5, 1140-1147.
16. N. S. Lynn and D. S. Dandy, *Lab on a Chip*, 2007, 7, 580-587.
17. M. S. Williams, K. J. Longmuir and P. Yager, *Lab on a Chip*, 2008, 8, 1121-1129.
18. S. Yun, G. Lim, K. H. Kang and Y. K. Suh, *Chem Eng Sci*, 2013, DOI: 10.1016/j.ces.2013.08.057.
19. J. Aubin, D. F. Fletcher and C. Xuereb, *Chem Eng Sci*, 2005, 60, 2503-2516.
20. J. D. Kirtland, G. J. McGraw and A. D. Stroock, *Physics of Fluids*, 2006, 18.
21. J. O. Foley, A. Mashadi-Hossein, E. Fu, B. A. Finlayson and P. Yager, *Lab on a Chip*, 2008, 8, 557-564.
22. J. P. Golden, T. M. Floyd-Smith, D. R. Mott and F. S. Ligler, *Biosensors & Bioelectronics*, 2007, 22, 2763-2767.
23. S. T. Wang, K. Liu, J. A. Liu, Z. T. F. Yu, X. W. Xu, L. B. Zhao, T. Lee, E. K. Lee, J. Reiss, Y. K. Lee, L. W. K. Chung, J. T. Huang, M. Rettig, D. Seligson, K. N. Duraiswamy, C. K. F. Shen and H. R. Tseng, *Angew Chem Int Edit*, 2011, 50, 3084-3088.
24. S. L. Stott, C. H. Hsu, D. I. Tsukrov, M. Yu, D. T. Miyamoto, B. A. Waltman, S. M. Rothenberg, A. M. Shah, M. E. Smas, G. K. Korir, F. P. Floyd, A. J. Gilman, J. B. Lord, D. Winokur, S. Springer, D. Irimia, S. Nagrath, L. V. Sequist, R. J. Lee, K. J. Isselbacher, S. Maheswaran, D. A. Haber and M. Toner, *Proceedings of the National Academy of Sciences of the United States of America*, 2010, 107, 18392-18397.
25. T. P. Forbes and J. G. Kralj, *Lab on a Chip*, 2012, 12, 2634-2637.
26. P. J. Roache, *Fundamentals of computational fluid dynamics*, Hermosa Publishers, Albuquerque, N.M., 1998.
27. R. B. Bird, W. E. Stewart and E. N. Lightfoot, *Transport phenomena*, J. Wiley, New York, 2nd, Wiley international edn., 2002.
28. N. S. Lynn, Biosensor Enhancement Using Grooved Micromixers: Part II, Experimental Studies, *simultanious submission*

For Table of Contents Only

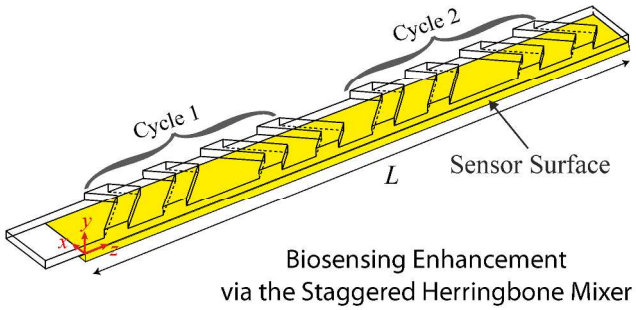

Biosensing Enhancement
via the Staggered Herringbone Mixer